

Tuning Rheochaos by Temperature in Wormlike Micelles

Rajesh Ganapathy and A. K. Sood*

Department of Physics, Indian Institute of Science, Bangalore 560012, India

Received July 26, 2006. In Final Form: September 20, 2006

We investigate the critical role played by the mean micellar length during the route to rheochaos for wormlike micellar gels of surfactant cetyltrimethylammonium tosylate in the presence of salt sodium chloride that show coupling of flow to concentration fluctuations. To this end, we have carried out stress/shear rate relaxation experiments at a fixed shear rate/stress but at different temperatures to take the sample through the route to rheochaos. We see the type-II intermittency route to rheochaos in stress relaxation measurements and the type-III intermittency route to rheochaos in shear rate relaxation measurements. We have also carried out linear rheology measurements at different temperatures to estimate the mean micellar length \bar{L} , the reptation time τ_{rep} , and the breaking time τ_{break} . It is shown that \bar{L} changes by $\approx 58\%$, as the sample goes through the route to rheochaos.

1. Introduction

Wormlike micelles are long semiflexible cylindrical aggregates of surfactant monomers, typically $\approx 1 \mu\text{m}$ in length and about $\approx 3\text{--}4 \text{ nm}$ in diameter and can relax stress through two mechanisms: reptation, analogous to polymers, and breaking and recombination.¹ The latter process of relaxing stress, not found in polymeric systems, leads to a plethora of novel flow behavior under modest external shear. One aspect in the nonlinear flow behavior of wormlike micelles that has attracted much attention in recent years is *shear banding*. For shear-thinning systems, above a critical shear rate, the stress decreases with further increase in the shear rate, and such a flow is mechanically unstable. The system therefore splits into high and low shear rate bands that coexist at a common stress. For shear-thickening systems, the reverse happens, and there exists high and low stress bands at a common shear rate. This phenomenon termed shear banding manifests itself as a plateau in the measured flow curve. Shear banding with a stable shear band interface was first predicted by Cates et al.² for shear-thinning wormlike micelles. However, there is surmounting experimental evidence showing the above picture to be inadequate. In many systems, shear banding is accompanied by aperiodic variation in the stress or shear rate in relaxation measurements. This phenomenon termed *rheochaos* occurs at practically zero Reynolds number and arises from the intrinsic nonlinearities in the viscoelastic equations. The phenomenon was first observed experimentally by Bandyopadhyay et al. in stress relaxation measurements for shear thinning wormlike micelles of surfactant cetyltrimethylammonium tosylate (CTAT).³ A thorough nonlinear time series analysis of the stress vs time data revealed the existence of deterministic chaotic dynamics. Since then rheochaos has been observed in a wide variety of other systems including shear-thickening wormlike micelles, lamellar and onion phases of surfactants, and dense colloidal suspensions.^{4–7} Recent experimental techniques such

as NMR velocimetry and optical measurements combined with conventional rheology to probe the shear band dynamics have shown that the band interface indeed shows complex spatio-temporal fluctuations, and this is accompanied by stress/shear rate fluctuations.^{8–11}

In theoretical models for rheochaos, spatial heterogeneity is a key ingredient. Chakrabarti et al.¹² have studied the spatio-temporal evolution of the traceless symmetric order parameter for a nematogenic fluid and have found chaos in a certain region of parameter space and the route to this chaos is via a regime of spatio-temporal intermittency.¹³ Cates et al.¹⁴ have proposed a phenomenological model for a shear-thickening fluid with memory and a tendency to form shear banded flows with one degree of freedom: shear stress. They have also studied a spatially inhomogeneous extension of this model, with spatial variation in the vorticity direction and find rich spatio-temporal behavior.¹⁵ The theoretical model of relevance to shear-thinning wormlike micelles is due to Fielding and Olmsted¹⁶ which takes into account the coupling of flow to the mean micellar length. By tuning the strength of this coupling, stable, intermittent, and chaotic shear banded states were seen.

In all shear rate/stress relaxation experiments reported so far, the stress/shear rate is the control parameter and the temperature is held fixed. Shear flow can influence the system in two ways: (i) it can either enhance breaking of the micelles or (ii) the end-to-end alignment of the micelles under flow can lead to elongation.¹⁷ The model by Fielding and Olmsted¹⁶ assumes the former. We may add that experimentally it is not clear which of the above occurs. Recently, Ganapathy et al.^{11,18} have shown that the route to chaos is via type-II intermittency in stress relaxation measurements and type-III intermittency in shear rate relaxation measurements for the shear thinning wormlike micellar

* Corresponding author. E-mail: asood@physics.iisc.ernet.in.

(1) Cates, M. E.; Candau S. J. *J. Phys.: Condens. Matter* **1990**, *2*, 6869.
 (2) Spenley, N. A.; Cates, M. E.; McLeish, T. C. B. *Phys. Rev. Lett.* **1993**, *71*, 939.
 (3) Bandyopadhyay, R.; Basappa, G.; Sood, A. K. *Phys. Rev. Lett.* **2000**, *84*, 2022.
 (4) Wunenburger, A. S.; Colin, A.; Leng, J.; Arnéodo, A.; Roux, D. *Phys. Rev. Lett.* **2001**, *86*, 1374.
 (5) Salmon, J.-B.; Manneville, S.; Colin, A. *Phys. Rev. E* **2003**, *68*, 051503.
 (6) Courbin, L.; Panizza, P.; Salmon, J.-B. *Phys. Rev. Lett.* **2004**, *92*, 018305.
 (7) Lootens, D.; van Damme, H.; Hébraud, P. *Phys. Rev. Lett.* **2003**, *90*, 178301.

(8) López-González, M. R.; Holmes, W. M.; Callaghan, P. T.; Photinos, P. *J. Phys. Rev. Lett.* **2004**, *93*, 268302.
 (9) Salmon, J.-B.; Manneville, S.; Colin, A. *Phys. Rev. E* **2003**, *68*, 051504.
 (10) Lerouge, S.; Argentina, M.; Decruppe, J. P. *Phys. Rev. Lett.* **2006**, *96*, 088301.
 (11) Ganapathy, R.; Majumdar, S.; Sood, A. K. Unpublished.
 (12) Chakrabarti, B.; Das, M.; Dasgupta, C.; Ramaswamy, S.; Sood, A. K.; *Phys. Rev. Lett.* **2004**, *92*, 055501.
 (13) Das, M.; Chakrabarti, B.; Dasgupta, C.; Ramaswamy, S.; Sood, A. K.; *Phys. Rev. E* **2005**, *71*, 021707.
 (14) Cates, M. E.; Head, D. A.; Ajdari, A. *Phys. Rev. E* **2002**, *66*, 025202.
 (15) Aradian, A.; Cates, M. E. *Euro. Phys. Lett.* **2005**, *70*, 397.
 (16) Fielding, S. M.; Olmsted P. D. *Phys. Rev. Lett.* **2004**, *92*, 084502.
 (17) Turner, M. S.; Cates, M. E. *J. Phys.: Condens. Matter* **1992**, *4*, 3719.
 (18) Ganapathy, R.; Sood, A. K. *Phys. Rev. Lett.* **2006**, *96*, 108301.

system of CTAT 2 wt % in the presence of salt sodium chloride (NaCl) which shows strong coupling of flow to concentration fluctuations. An important thing to note is that the theoretical model by Fielding and Olmsted predicts a Hopf bifurcation¹⁹ in stress relaxation essential for observing the Type-II intermittency route to chaos. Given the strong similarities between theoretical predictions and experimental observations, it is natural to ask the role played by the coupling of flow to the micellar length in an experimental system. It is well-known that the mean micellar length is extremely sensitive to temperature and decreases with increase in temperature.¹ In this paper, we have carried out stress/shear rate relaxation measurements at a fixed shear rate/stress with temperature as the control parameter and thereby control the micellar length. We find that shear leads to elongation of micelles during the route to rheochaos.

2. Background

The nonlinear flow behavior of CTAT 2 wt % at different NaCl concentration was first addressed by Bandyopadhyay and Sood.²⁰ It was found that the slope α of the plateau in the flow curve ($\sigma \sim \dot{\gamma}^\alpha$) can be tuned by the addition of salt NaCl. This slope is attributed to a concentration difference between the shear bands^{18,21} arising from the Helfand–Fredrickson mechanism.²² Here, the high shear rate band is predicted to be lower in concentration due to micelles diffusing against their own concentration gradients leading to flow-enhanced concentration fluctuations. Small angle light scattering measurements performed under flow showed a “butterfly” light scattering pattern with the wings of the butterfly stretched along the flow direction^{23,24} for salt concentrations $25 \text{ mM} < c_{\text{NaCl}} < 1 \text{ M}$, corresponding to plateau slopes $0.12 < \alpha < 0.4$, confirming the Helfand–Fredrickson scenario. Also all systems that showed a “butterfly” light scattering in SALS measurements also showed the type-II intermittency route to rheochaos in stress relaxation measurements¹⁸ and the type-III intermittency route to rheochaos in shear rate relaxation measurements.¹¹

There are primarily three routes to chaos: the period-doubling route, the quasiperiodic route and the intermittency route. The intermittency route is mainly characterized by bursts of chaos disrupting nearly periodic (laminar region) oscillations. Pomeau and Manneville²⁵ have established that within the intermittency route there are further three types. Type-I appears with an inverse tangent bifurcation, type-II with a Hopf bifurcation and type-III with a period doubling bifurcation.

3. Experimental Section

The phase behavior of cetyltrimethylammonium tosylate [CTAT] has been well characterized by Soltero et al.²⁶ Above the Krafft temperature of 23 °C and at low surfactant concentrations $c < 0.04 \text{ wt } \%$, spherical micelles are formed. At higher concentrations ($0.04 \text{ wt } \% < c < 0.4 \text{ wt } \%$), cylindrical micelles are formed which, at $c > c^* = 0.4 \text{ wt } \%$, entangle to form viscoelastic gels. CTAT (Sigma Aldrich, 98%) was used without further purification. The CTAT/NaCl/water samples were prepared by dissolving known amounts of CTAT in water and brine (100 mM), respectively. The samples were then filtered through 200 nm pore size filters to remove dust impurities and left to equilibrate for 2–3 days. The experiments

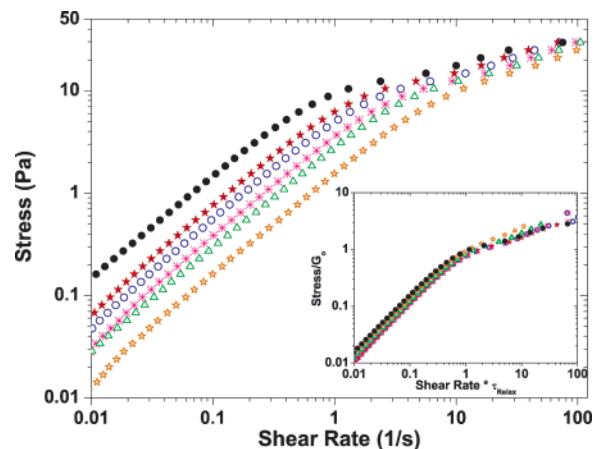


Figure 1. Stress controlled flow curves for the CTAT 2 wt % + 100 mM NaCl at different temperatures. $T = 34 \text{ }^\circ\text{C}$ (hollow stars), $T = 31 \text{ }^\circ\text{C}$ (hollow triangles), $T = 29.5 \text{ }^\circ\text{C}$ (crosses), $T = 28 \text{ }^\circ\text{C}$ (hollow circles), $T = 26.5 \text{ }^\circ\text{C}$ (filled stars), and $T = 24 \text{ }^\circ\text{C}$ (solid circles). Inset: Flow curves rescaled by plateau modulus G_0 and relaxation time τ .

were carried out on a MCR 300 rheometer (Anton PAAR) in the cylindrical Couette geometry (Inner Cylinder dia. 16 mm, Outer cylinder dia. 18 mm, Height 16.5 mm). A water circulator was used for temperature control of the Couette cell to an accuracy of $\pm 0.1 \text{ }^\circ\text{C}$.

The flow curves were performed under controlled-stress conditions. The waiting time per data point was 60 s. The stress/shear rate relaxation experiments were carried out by applying a step shear rate/stress at $t = 0 \text{ s}$, and the resulting stress/shear rate was recorded as a function of time using the US 200 rheometer control software (Anton PAAR). The data points were measured at 0.5 s intervals. The data analysis including Fourier transforms were performed using the Origin 6.1 (OriginLab Corp., U.S.A.) data analysis and plotting software.

4. Results and Discussions

Figure 1 shows the flow curves at different temperatures for the CTAT 2 wt % + 100 mM NaCl sample in a controlled-stress experiment. After the initial Newtonian regime, all of the flow curves show a plateau with a finite slope, $0.3 < \alpha < 0.35$, for temperatures T ranging from $24 \text{ }^\circ\text{C} < T < 34 \text{ }^\circ\text{C}$. This value of the plateau slope is in good agreement with earlier reported values for the same system¹⁸ and implies strong coupling of flow to concentration fluctuations. This is corroborated by the visual observation of the “butterfly” intensity pattern in small angle light scattering measurements.¹⁸ The inset to Figure 1 shows the flow curves at various temperatures normalized by the plateau modulus G_0 and the terminal relaxation time τ_R determined from linear rheology experiments described later. All of the flow curves collapse on a master curve, and this suggests that the temperature does not play an important role in altering the strength of the coupling between flow and concentration fluctuations.

4.1. Stress Relaxation Measurements. Figure 2 shows the results of stress relaxation measurements done at a fixed shear rate, $\dot{\gamma} = 25 \text{ s}^{-1}$, and at various temperatures. The initial transients are not shown. Figure 2a shows data of stress relaxation done at $T = 31.5 \text{ }^\circ\text{C}$. The stress remains flat and does not show any time dependence. In Figure 2b for $T = 28.8 \text{ }^\circ\text{C}$, the stress shows oscillations. In Figure 3a, the Fourier power spectrum of this time series is shown. We see a primary frequency centered around $\omega = 0.032 \text{ Hz}$ and its higher harmonics revealing the periodic nature of the oscillations. At a slightly lower temperature of $T = 27.2 \text{ }^\circ\text{C}$ the stress oscillations become more complex and look like a beat pattern (Figure 2c). A Fourier power spectrum of this

(19) Ott, E. *Chaos in Dynamical Systems*; Cambridge University Press: Cambridge, 1993.

(20) Bandyopadhyay, R.; Sood, A. K. *Langmuir* **2003**, *19*, 3121.

(21) Fielding, S. M.; Olmsted, P. D. *Eur. Phys. J. E.* **2003**, *11*, 65.

(22) Helfand, E.; Fredrickson, G. H. *Phys. Rev. Lett.* **1989**, *62*, 2468.

(23) Kadoma, I. A.; van Egmond, J. W. *Phys. Rev. Lett.* **1996**, *76*, 4432.

(24) Kadoma, I. A.; van Egmond, J. W. *Phys. Rev. Lett.* **1998**, *80*, 5679.

(25) Pomeau, P.; Manneville, P. *Commun. Math. Phys.* **1980**, *74*, 189.

(26) Soltero, J. F. A.; Puig, J. E. *Langmuir* **1995**, *11*, 3337.

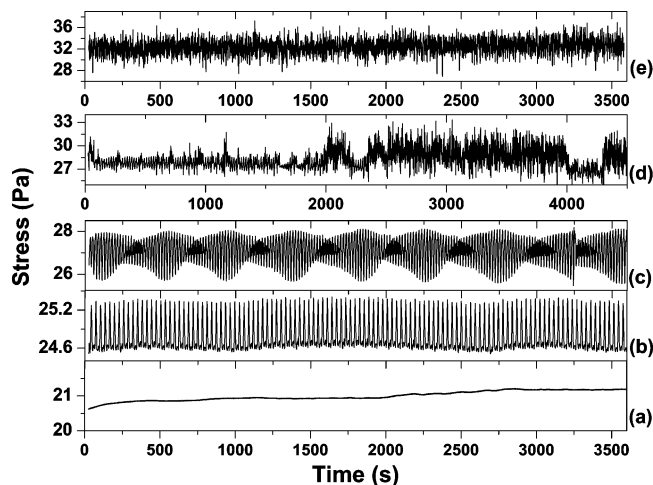


Figure 2. Stress relaxation time series at fixed $\dot{\gamma} = 25s^{-1}$ and at different temperatures. (a) $T = 31.5$ °C, (b) $T = 28.8$ °C, (c) $T = 27.2$ °C, (d) $T = 26.5$ °C, and (e) $T = 26$ °C.

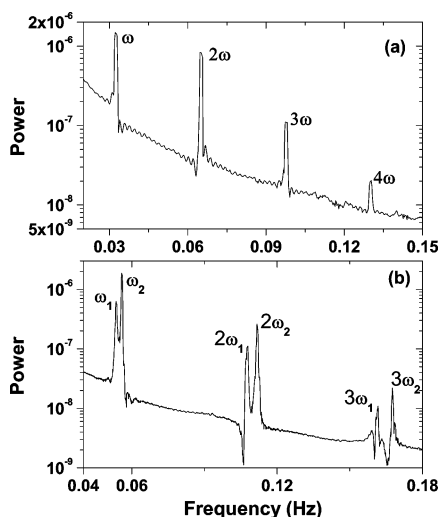


Figure 3. (a) Fourier power spectrum of data shown in Figure 2b. (b) Fourier power spectrum of data shown in Figure 2c.

signal (Figure 3b) shows the presence of two primary frequency components centered around $\omega_1 = 0.053$ Hz and $\omega_2 = 0.055$ Hz and their higher harmonics. The signal is therefore quasiperiodic.^{18,19} Figure 2d shows the stress relaxation dynamics for $T = 26.5$ °C. The signal shows laminar (nearly periodic) regions and intermittent chaotic bursts. Figure 4a shows an expanded plot of the data shown in Figure 2d. The nature of the signal during the laminar phase rules out type-III intermittency, since, for this type of intermittency, there should be a subharmonic mode with increasing amplitude. One standard test for intermittent time series is to look at the probability distribution of laminar lengths between burst events.²⁷ Figure 4b shows the histogram of the laminar length probability distribution, and the thick solid line shows the fit to an exponential decay expected for type-II intermittency at long times.^{18,27} Another standard test for analyzing type-II intermittency is by constructing Poincaré return maps for the laminar regions between bursts. We are unable to carry out this test due to the extremely short laminar regions between the chaotic bursts. Figure 2e shows the stress relaxation dynamics at $T = 26$ °C. A time series analysis of this data is not possible since the time series shows high dimensional chaos with a correlation dimension $\nu > 8$ and an extremely long time series

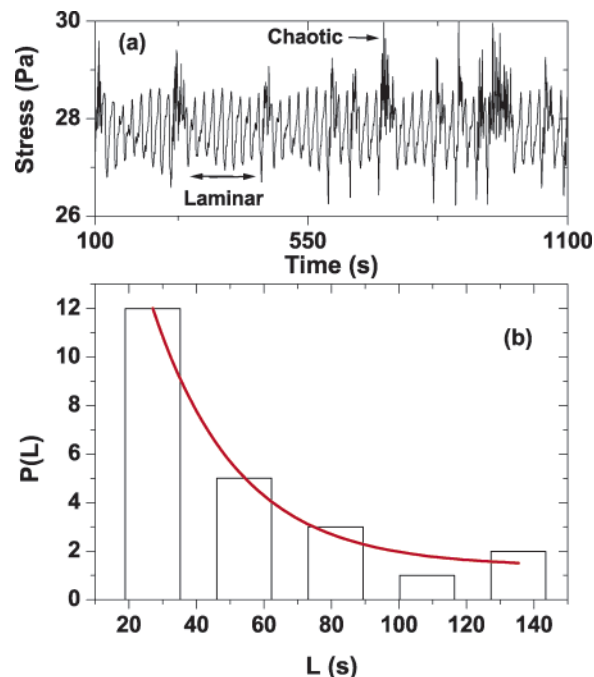


Figure 4. (a) Expanded plot of data shown in Figure 2d. (b) Probability distribution of laminar lengths. The line shows the exponential fit to the data.

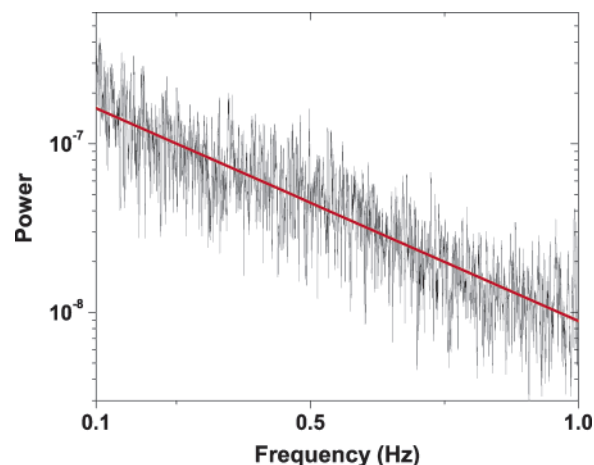


Figure 5. Fourier power spectrum of data shown in Figure 2e. The red line is the fit.

would be required to show that the data is deterministic. However, the power spectrum of the data shown in Figure 5 shows that the power spectrum decays exponentially, signifying the presence of deterministic chaos.^{28,29}

4.2. Shear Rate Relaxation Measurements. Figure 6 shows the results of the shear rate relaxation measurements done at a fixed stress, $\sigma = 33$ Pa, and at various temperatures after removing the initial transients. Figure 6a shows the results of shear rate relaxation at $T = 37$ °C. This time series does not reveal any time dependence. Figure 6b shows the results of shear rate relaxation for $T = 32.5$ °C. Initially the data shows features characteristic of type-III intermittency, which we describe below in detail, and after about 3900 s the oscillations become periodic. This change in the nature of the oscillations could be due to the presence of an extremely slow transient in the system.³⁰ Type-III intermittency

(28) Greenside, H. S.; Ahlers, G.; Hohenberg, P. C.; Walden, R. W. *Physica D* **1984**, *5*, 322.

(29) Brandsatter, A.; Swinney, H. L. *Phys. Rev. A* **1987**, *35*, 2207.

(30) Bécú, L.; Manneville, S.; Colin, A. *Phys. Rev. Lett.* **2004**, *93*, 018301.

(27) Schuster, H. G. *Deterministic Chaos*; VCH: Weinheim, Germany, 1988.

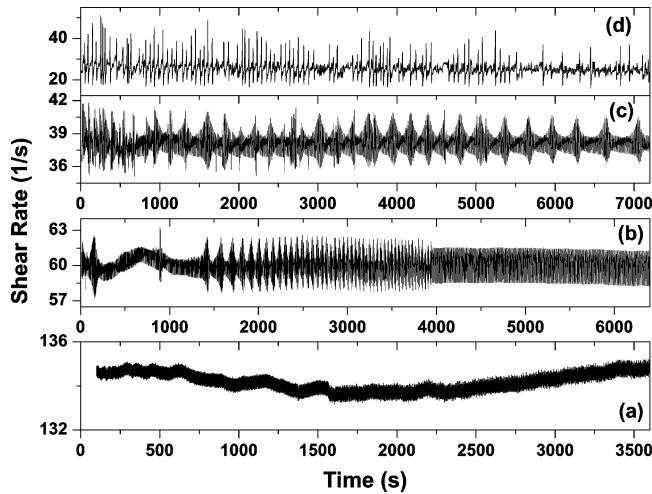


Figure 6. Shear rate relaxation time series at fixed $\sigma = 33$ Pa and at different temperatures. (a) $T = 37$ °C, (b) $T = 32.5$ °C, (c) $T = 30$ °C, and (d) $T = 27.5$ °C.

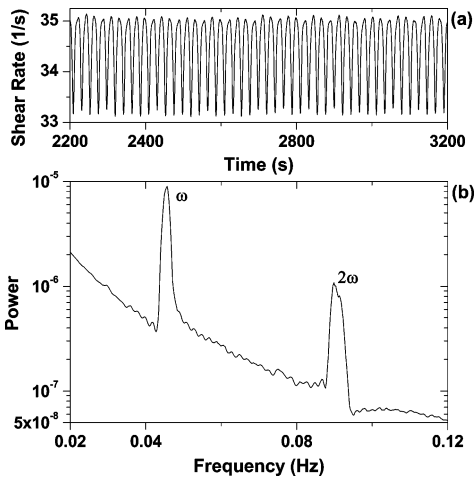


Figure 7. (a) Shear rate relaxation time series at fixed $\sigma = 28$ Pa and at $T = 29.5$ °C. (b) Fourier power spectrum of (a).

is preceded by a period-doubling bifurcation¹⁹ and in this run, we did not see simple periodic behavior. Figure 7a shows the time series for a repeat run done at a different stress, $\sigma = 28$ Pa, and at $T = 29.5$ °C. Figure 7b shows the Fourier power spectrum of these data. The data are periodic as shown by the presence of a primary frequency component centered around $\omega = 0.045$ Hz and its higher harmonic. At lower temperatures, shear rate relaxation data for this stress ($\sigma = 28$ Pa) was similar to the ones shown in Figure 6 ($\sigma = 33$ Pa). Figure 6c shows the shear rate time series at $T = 30$ °C. An expanded plot of these data is shown in Figure 8a. The signal shows laminar regions interspersed with turbulent bursts. There are two frequency components, ω_0 and $\omega_0/2$, which we call the fundamental and the sub-harmonic mode, respectively. The amplitude of the fundamental mode decreases, and this is accompanied by a simultaneous increase in the amplitude of the sub-harmonic mode. When the sub-harmonic mode reaches a critical value, the signal loses all regularity and a turbulent burst appears. This is followed by the reappearance of the laminar behavior. This kind of behavior is typical of Type-III intermittency.³¹ To be more quantitative, we reconstruct a Poincaré second return map to analyze the data. In Figure 8b, we plot the successive maxima of the subharmonic mode (shown by circles) and the decreasing amplitude of the fundamental

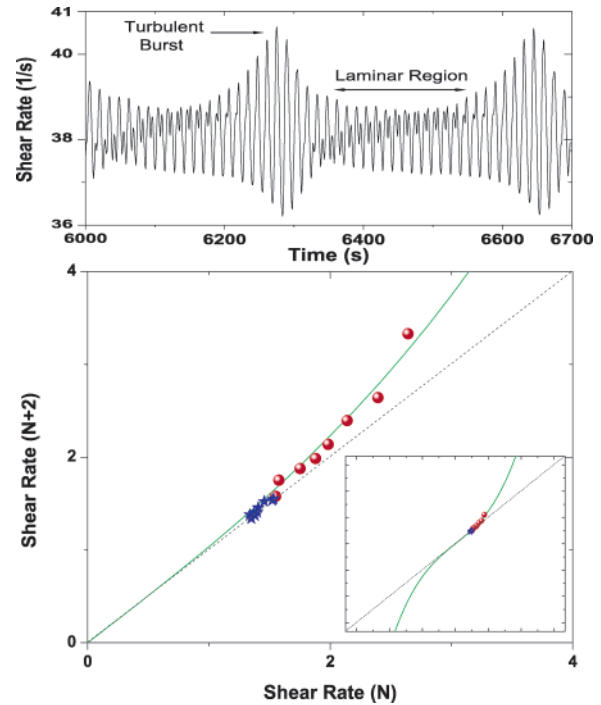


Figure 8. (a) Expanded plot of data shown in Figure 6c. (b) Poincaré return map of the data shown in (a). Circles denote the increasing amplitude of the subharmonic mode and stars denote the decreasing amplitude of the fundamental mode. The continuous line shows the fit to the experimental data.

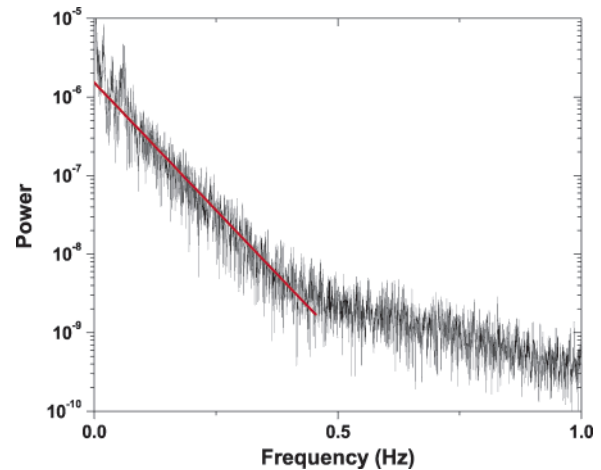


Figure 9. Fourier power spectrum of data shown in Figure 6d. The red line is the fit.

mode (shown by stars) for the data in the laminar region of Figure 8a. For type-III intermittency preceded by a period-doubling bifurcation the return map can be expressed as follows: $A_{n+2} = (1 + 2\epsilon)A_n + aA_n^3$, where ϵ is proportional to the control parameter (temperature in our experiments), a is a constant, and A_n are the maxima of the sub-harmonic or the fundamental mode.³² The green line (Figure 8b) shows the fit of the above expression to experimental data which yields $\epsilon = 0.004$. At a lower temperature, $T = 27.5$ °C, the data is chaotic as characterized by the exponential decay of the Fourier power spectrum (Figure 9).

4.3. Linear Rheology Measurements. The results of the above measurements with temperature as the control parameter show the type-II intermittency and type-III intermittency route to rheochaos in stress and shear rate relaxation, respectively. These

(31) Dubois, M.; Rubio, M. A.; Berge, P. *Phys. Rev. Lett.* **1983**, *51*, 1446.

(32) Bergé, P.; Pomeau, Y.; Vidal, B. *Order Within Chaos*; Hermann: Paris, 1984.

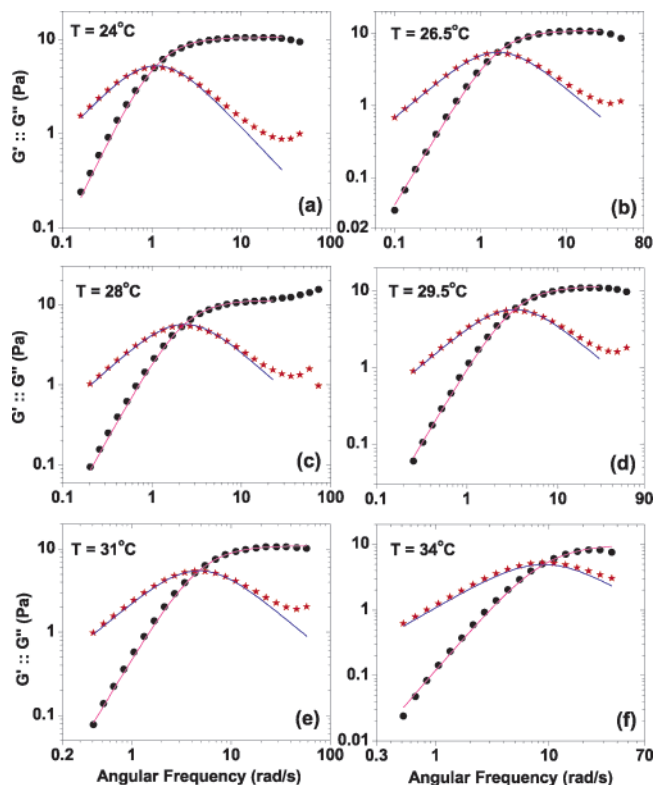


Figure 10. Frequency sweep measurements at different temperatures. $G'(\omega)$ is shown by solid circles and $G''(\omega)$ shown by stars. The lines are fits using a Maxwell model

results are similar to the earlier measurements on the same sample with shear rate and stress as the control parameter.^{11,18} We will now show that the role of temperature in the present experiments is to increase the mean micellar length when the sample goes through the route to rheochaos. To quantify this, we have carried out frequency sweep measurements from which the breaking time and the mean micellar length can be determined. We would like to mention here that the stress/shear rate relaxation experiments are done in the nonlinear domain whereas the frequency sweep measurements, from which the mean micellar length is estimated, are done in the linear domain. Hence the absolute values of the mean micellar length may be modified, but we believe that the change in the micellar length, which shows an increase, will remain unchanged. We describe below the results of the linear rheology measurements.

Figure 10 shows the results of the frequency sweep measurements done at various temperatures $24\text{ }^\circ\text{C} < T < 34\text{ }^\circ\text{C}$. The storage modulus $G'(\omega)$ and the loss modulus $G''(\omega)$ are shown by circles and stars, respectively. The continuous lines are the fits to a Maxwell model with a single relaxation time:

$$G'(\omega) = \frac{G_0 \omega^2 \tau^2}{1 + \omega^2 \tau^2} \quad (1)$$

$$G''(\omega) = \frac{G_0 \omega \tau}{1 + \omega^2 \tau^2} \quad (2)$$

where G_0 is the plateau modulus and τ is the terminal relaxation time. The fits are excellent in the range of temperatures studied. For Maxwellian behavior, the terminal relaxation time $\tau = (\tau_{\text{break}} \tau_{\text{rep}})^{1/2}$.³³ This implies that $\tau_{\text{break}} < \tau_{\text{rep}}$, where τ_{break} and τ_{rep}

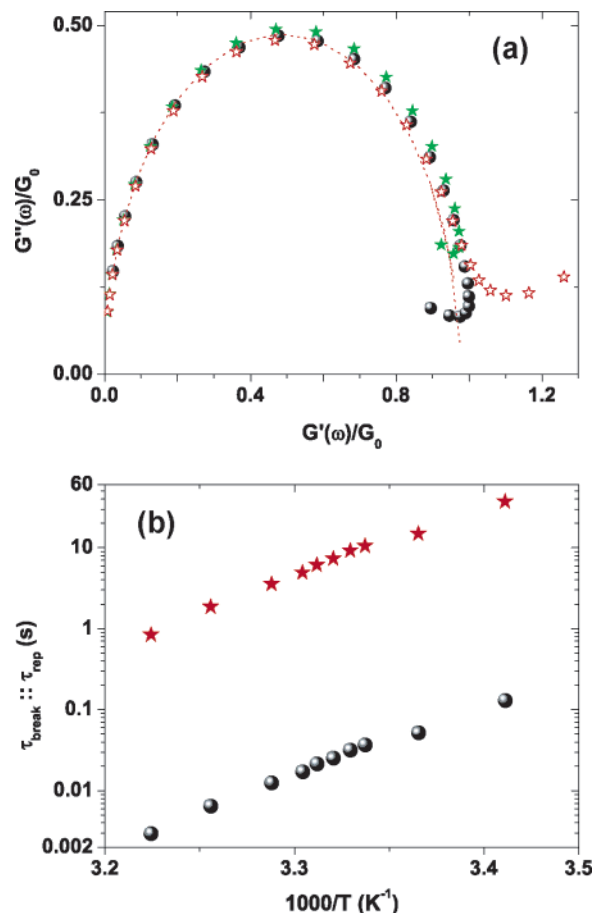


Figure 11. (a) Cole–Cole representation of the frequency sweep measurements at different temperatures. $T = 31\text{ }^\circ\text{C}$ (solid stars), $T = 28\text{ }^\circ\text{C}$ (hollow stars), and $T = 24\text{ }^\circ\text{C}$ (solid circles). (b) τ_{break} (circles) and τ_{rep} (stars) plotted against inverse temperature.

Table 1. Temperature Dependence of Parameters Estimated from Linear Rheology Data

T (K)	G_0 (Pa)	G''_{Min}/G_0	τ (s)	τ_{break} (s)	τ_{rep} (s)	\bar{L} (nm)
293.15	10.9	0.05	2.2	0.129	37.28	3364
297.15	10.5	0.08	0.88	0.051	14.91	2254
299.65	10.9	0.10	0.62	0.036	10.50	1795
300.35	11.0	0.10	0.54	0.031	9.15	1785
301.15	11.3	0.11	0.43	0.025	7.28	1653
301.95	11.3	0.13	0.36	0.021	6.10	1417
302.65	11.4	0.14	0.29	0.017	4.91	1323
304.15	10.9	0.16	0.21	0.012	3.55	1135
307.15	9.8	0.28	0.11	0.006	1.86	667
310.15	9.4	0.39	0.05	0.002	0.84	475

are the breaking and reptation time of the micelles, respectively.³³ The fits yield G_0 and τ . In Figure 11a, the frequency sweep measurements are shown in a Cole–Cole representation. The plot is semicircular and the data obtained at various temperatures overlap. Using the procedure due to Turner and Cates,³⁴ we fit the Cole–Cole data to a circle subject to the constraint that it passes through the origin and the center of the circle lies on the $G'(\omega)$ axis. The data from numerical simulations helps us to relate the diameter of the fitted circle to $\bar{\zeta}$, where $\bar{\zeta} = (\tau_{\text{break}}/\tau)$.³⁴ The diameter of the fitted circle for the experimental data is found to be 0.97 corresponding to $\bar{\zeta} = 0.059$. Figure 11b shows the Arrhenius dependence of the τ_{break} and τ_{rep} with temperature. The values of different parameters estimated from the frequency sweep measurements are shown in Table 1.

(33) Cates, M. E. *Macromolecules* **1987**, *20*, 2289.

(34) Turner, M. S.; Cates, M. E. *Langmuir* **1991**, *7*, 1590.

The frequency sweep measurements at various temperatures show a minimum in $G''(\omega)$ followed by an increase. This is due to the presence of Rouse modes with frequencies corresponding to the chain motion between entanglements. The value of G''_{Min} is related to the chain length by

$$G''_{\text{Min}} G_0 = A l_e \bar{L} \quad (3)$$

Here A is a constant of order unity and l_e is the entanglement length. For flexible wormlike chains, l_e is related to G_0 by^{35–37}

$$G_0 \sim \frac{k_B T}{l_e^{9/5}} \quad (4)$$

where k_B is the Boltzmann constant and T is the temperature.

Using the above relations, we estimate the value of the mean micellar length \bar{L} at various temperatures for the CTAT 2 wt % + 100mM NaCl system (Table 1). Figure 12 shows the log-linear plot of mean micellar length against an inverse temperature. The plot is linear showing that the micellar length and temperature are related by an Arrhenius relation. The micellar length increases by $\approx 58\%$ for $31^\circ\text{C} > T > 26^\circ\text{C}$, the region in temperature over which we see the route to rheochaos.

5. Conclusions

To conclude, we have shown for the first time that the route to rheochaos in wormlike micellar gels can be tuned by varying the temperature in stress/shear rate relaxation experiments carried out at a fixed shear rate/stress. We see the type-II intermittency and the type-III intermittency route to rheochaos in stress and

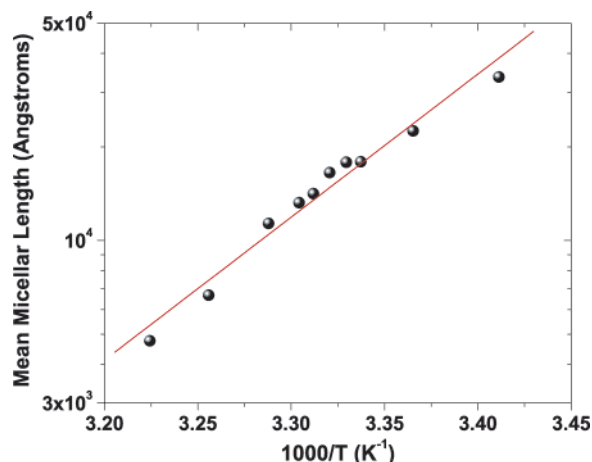


Figure 12. Mean micellar length plotted against inverse temperature.

shear rate relaxation experiments, respectively. These results are similar to the routes to rheochaos seen with stress/shear rate as the control parameter at a fixed temperature. This implies that in our experiments with shear rate and stress as the control parameter, there may be an elongation in the mean micellar length when the sample goes through the route to rheochaos. Like in the theoretical prediction,¹⁶ we see a strong coupling of flow to the mean micellar length. We find that the strength of this coupling does not alter with temperature. We see that flow induces an increase in the mean micellar length due to an end-to-end alignment of the wormlike chains. At the moment, a complete theoretical understanding of rheochaos seen in wormlike micelles and other complex fluids is lacking. We believe that our experiments will provide a firm testing ground for future theories to come.

(35) Doi, M.; Edwards, S. F. *The Theory of Polymer Dynamics*; Clarendon: Oxford, 1986.

(36) Soltero, J. F. A.; Puig, J. E.; Manero, O. *Langmuir* **1996**, *12*, 2654.

(37) Kern, F.; Lequeux, F.; Zana, R.; Candau, S. J. *Langmuir* **1994**, *10*, 1714.